J. Water Environ. Nanotechnol., 8(1): 13-22 Winter 2023

ORIGINAL RESEARCH PAPER

Synthesis of p-n heterojunction photocatalyst from ZnO nanorod and Cu_2O nanoparticles for visible light photocatalytic degradation of Paraoxon insecticide

Ghader Hosseinzadeh [1,*]

[1] *Department of Chemical Engineering, University of Bonab, Bonab, Iran.*

Received: 2022-10-12 Accepted: 2022-12-08 Published: 2023-02-10

ABSTRACT

In the current work, a novel ZnO-Cu_2O heterojunction was synthesized from ZnO nanorods and Cu_2O nanoparticles via a hydrothermal route and was applied for the first time as a visible light-active photocatalyst for the Paraoxon insecticide decomposition. Crystallinity, shape, and size of the particles and optical properties of the synthesized heterojunction nanocomposites were evaluated by XRD, FESEM, EDS, Mott-Schottky, photocurrent analysis, and UV-Visible spectroscopy analyses. Based on the obtained results, the ZnO-Cu_2O heterojunction nanocomposite was successfully synthesized and compared to pure ZnO semiconductor has enhanced photocatalytic efficiency. The nanocomposite with a 40% weight percentage of Cu_2O has the best photocatalytic activity of 0.0201 min^{-1}, which could be related to the improvement of optical properties (the increase in the visible light harvesting ability) and the recombination reduction of the photoinduced electron-hole pairs. In addition, according to the radical trapping tests and Mott-Schottky experiments, superoxide radical was determined as the main oxidizing species for the photocatalytic degradation of Paraoxon, and a type II charge transfer process was proposed for the improved photocatalytic activity.

Keywords: ZnO, Cu_2O; Nanocomposite; Type II; Paraoxon

How to cite this article

Hosseinzadeh G., Synthesis of p-n heterojunction photocatalyst from ZnO nanorod and Cu_2O nanoparticles for visible light photocatalytic degradation of Paraoxon insecticide. J. Water Environ. Nanotechnol., 2023; 8(1): 13-22

DOI: 10.22090/jwent.2023.08.002

INTRODUCTION

Paraoxon is one of the most important commercial organophosphate insecticides due to its high insecticidal efficiency, wide range of applications, and sufficient solubility in water. Nevertheless, due to its wide use in agriculture, it is commonly recognized as an environmental pollutant in surface water, soil, and groundwater [1]. In this regard, advanced technologies including microbial degradation, the use of nanomembrane, and photocatalytic decomposition have been developed for the removal of insecticides from contaminated environments [2-4]. Among the mentioned technologies, photocatalytic decomposition of the insecticides has some merits including [5, 6].

* Corresponding Author Email: *g.hosseinzadeh@ubonab.ac.ir*

ZnO is a widely used semiconductor photocatalyst, which has a wide application in the photocatalytic degradation of different pollutants. The major advantages of ZnO are its good chemical stability, non-toxicity, low production cost, and high eco-friendly [7, 8]. However, it has a high energy band-gap value, and low visible light photocatalytic activity, furthermore, the fast recombination of photogenerated electrons and holes remarkably reduces its photocatalytic performance [9]. Therefore, to solve these problems and to improve the visible light photocatalytic efficiency of ZnO, different techniques have been developed in recent years such as doping [10], surface modification [11], morphology manipulation [12], defect engineering [13], and formation of hybrids and heterojunctions [9]. Among the above strategies, coupling of ZnO

with other semiconductors in the heterojunction composite form has gained considerable interest, due to the potential capability of this method to enhance the photocatalytic activity via extending the visible-light harvesting and suppression of the recombination of the photogenerated electron–hole pairs. In this regard, various heterojunction photocatalysts of ZnO have been prepared such as $ZnO/ZnBi_2O_4$ [14], ZnO/CuO [15], ZnO/MoS_2[16], $ZnO/g\text{-}C_3N_4$ [17], ZnO/Bi_2MoO_6 [18], and Ag_2O/ZnO [19].

During the past decades, the p-type Copper (I) oxide (Cu_2O) semiconductor has gained remarkable consideration as a promising photocatalyst for the photocatalytic decomposition of various pollutants [20]. Nevertheless, it has a narrow band gap, and because of the fast recombination of the photoinduced electron–hole pairs on its surface, Cu_2O has low photocatalytic efficiency. In order to overcome this restriction, various techniques have been studied for the reduction of the charge carriers recombination on this semiconductor, one of the most promising strategies is the compositing of Cu_2O with other semiconductors in heterojunction form, such as TiO_2/Cu_2O [21], Ag_2O/Cu_2O [22], Cu_2O/Bi_2S_3 [23], Fe_2O_3/Cu_2O [24], $Cu_2O/Cu_2V_2O_7$ [25], and $SrTiO_3/Cu_2O$ [26].

In the current study, ZnO-Cu_2O heterojunction photocatalyst was produced by an innovative hydrothermal method from ZnO nanorods, and Cu_2O nanoparticles and was applied as a visible light active photocatalyst for the degradation of Paraoxon insecticide. Based on the literature review, there is no report on the construction of ZnO-Cu_2O heterojunctions with nanorods and nanoparticles morphologies; in addition, there is no published article about the usage of ZnO-Cu_2O photocatalyst for the degradation of Paraoxon insecticide. The prepared photocatalysts were characterized by XRD, EDS, FESEM, Mott-Schottky, photocurrent, and DRS analysis.

EXPERIMENTAL

Materials

$Zn(NO_3)_2.6H_2O$, Ethylene glycol, Na_2CO_3, ammonia solution (25%), ethanol, Copper(II) nitrate trihydrate, Glycine, Potassium hydroxide were purchased in analytical grade from Merck, Germany, and were used as raw materials without any purification.

Synthesis of ZnO nanorods

To prepare ZnO nanorods, 1.5 g of zinc nitrate hexahydrate and 3 ml of were dissolved in 50 ml then 0.5 g of sodium carbonate was added and stirred for 2 hours. The resulting solution was transferred into a Teflon-lined stainless autoclave and subjected to a hydrothermal process at 120 °C for 12 hours. The final precipitates were immediately separated by centrifugation, washed with water and ethanol, and dried at 80°C. In this method, sodium carbonate was used as a weak base for the shape-controlled conversion of zinc cations to ZnO nanorods which were converted to CO_2 gas during the hydrothermal process.

Synthesis of Cu2O nanoparticles

To synthesize Cu_2O nanoparticles, 1.21 g of Copper (II) nitrate trihydrate was dissolved in 50 ml deionized water, and in another beaker, 0.75 g of Glycine amino acid was dissolved in 50 ml deionized water. These two solutions were mixed and under ultrasonication, 0.56 g Potassium hydroxide was added to the mixed solution. Later on, the solution was poured into a Teflon-lined stainless autoclave and was subjected to the hydrothermal process for 5 hours at a temperature of 200 °C. The resulting nanoparticles were separated by centrifugation, washed with water and ethanol, and dried at 80°C.

Synthesis of ZnO-Cu_2O nanocomposite

In a typical procedure, for the preparation of ZnO-Cu_2O heterojunction photocatalyst with 10, 20, 30, 40, and 50% weight percentage of Cu_2O nanoparticles, which are labeled as ZnO-10Cu2O, ZnO-20Cu2O, ZnO-30Cu2O, ZnO-40Cu2O, and ZnO-50Cu2O, desired amounts of the prepared ZnO nanorods was fully dispersed by probe ultrasonication in the final solution of Cu_2O as described in the above section. At that point, the final suspension was poured into Teflon lined stainless autoclave and subjected to the hydrothermal process for 5 h at a temperature of 200 °C. After completing the process, the prepared samples were extracted by centrifuge, and after washing with deionized water and ethanol, dried at 80 °C.

Photocatalytic activity

The photocatalytic efficiencies of the synthesized samples were investigated by measuring the degradation of Paraoxon insecticide under visible light irradiation. A 570W Xenon lamp equipped

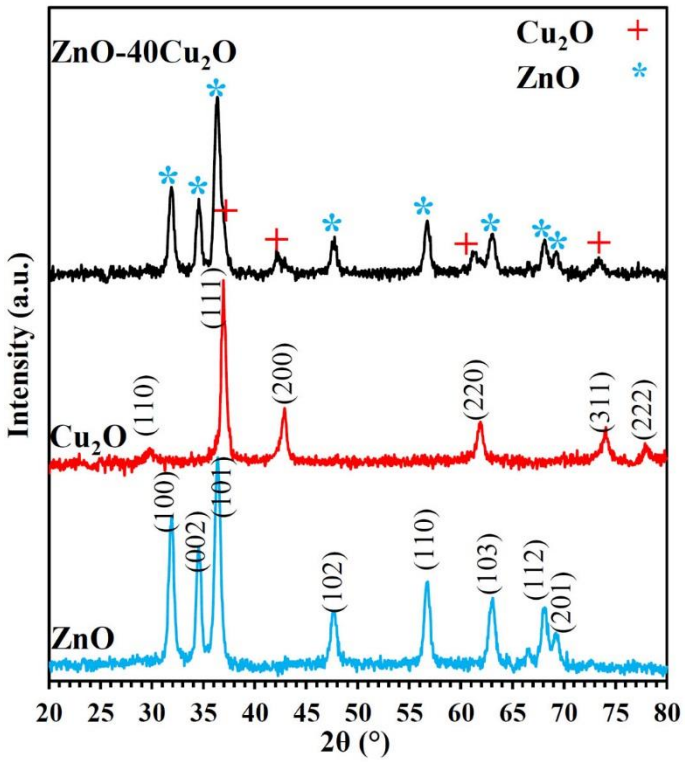

Fig. 1. XRD patterns of the prepared samples.

with an L41 UV-cut-off filter (Kenko Co.) was used as a visible light source. Briefly, 50 mg of photocatalyst sample was fully dispersed in 100 mL of the aqueous solution of Paraoxon with the initial concentration of 30 mg/L. The resulting suspension was maintained under dark conditions and stirred for 4 h to reach an adsorption–desorption equilibrium, and afterward was irradiated at the pH level of 7 and temperature of 25 °C. Every 15 min, 5 mL of aliquot was sampled and immediately centrifuged to deposit the remnant photocatalyst nanocomposites, and the remaining concentration of Paraoxon insecticide was measured via Cary 100 Bio UV–Vis spectrophotometer.

RESULTS AND DISCUSSION

The crystal structure of the synthesized samples was characterized by X-ray diffraction (XRD) using a Philips X'Pert MPD X-ray diffractometer (Netherlands) with Cu Kα radiation (λ = 1.54056 Å). In Fig. 1, for the ZnO nanorods, the major diffraction peaks positioned at 2θ = 31.9°,34.7°, 36.5°, 47.9, 56.8°, 62.9°, 68.1°, and 69.3° can be respectively assigned to (100), (002), (101), (102), (110). (103), (112), and (201) lattice planes of the hexagonal phase of ZnO (JCPDS # 80-0074) [27]. In the graph of Cu_2O nanoparticles, the peaks at 2θ = 29.9°,37.8°, 42.9°, 61.9, 74.1°, and 78.1° can be assigned to the (110), (111), (200), (220), (311) and (222) planes respectively, corresponding to the cubic Cu_2O structure (JCPDS 65-3288) [28]. In the XRD graph of the ZnO-Cu_2O heterojunction sample, the diffraction lines of ZnO and Cu_2O are seen, indicating the victorious synthesis of the heterojunction nanocomposite. Broadening of the XRD lines indicates the nanostructure nature of the prepared samples and the estimated crystallite sizes based on Debye-Scherrer's formula [29] for the ZnO and Cu_2O samples are about 18 nm and 20 nm, respectively.

The FE-SEM experiment using Tescan MIRA 3 FESEM (Czech Republic), was used to investigate the size and morphology of the prepared nanostructures. The FE-SEM images of the synthesized ZnO-40Cu2O heterojunction are seen in Figs. 2A and B. In this image, the ZnO nanorods with an approximate diameter of 50-70 nm can be observed, and Cu_2O nanoparticles are also seen in this image. The difference between particle size approximated from Debye-Scherrer's equation and that of the FE-SEM images is mainly related to the

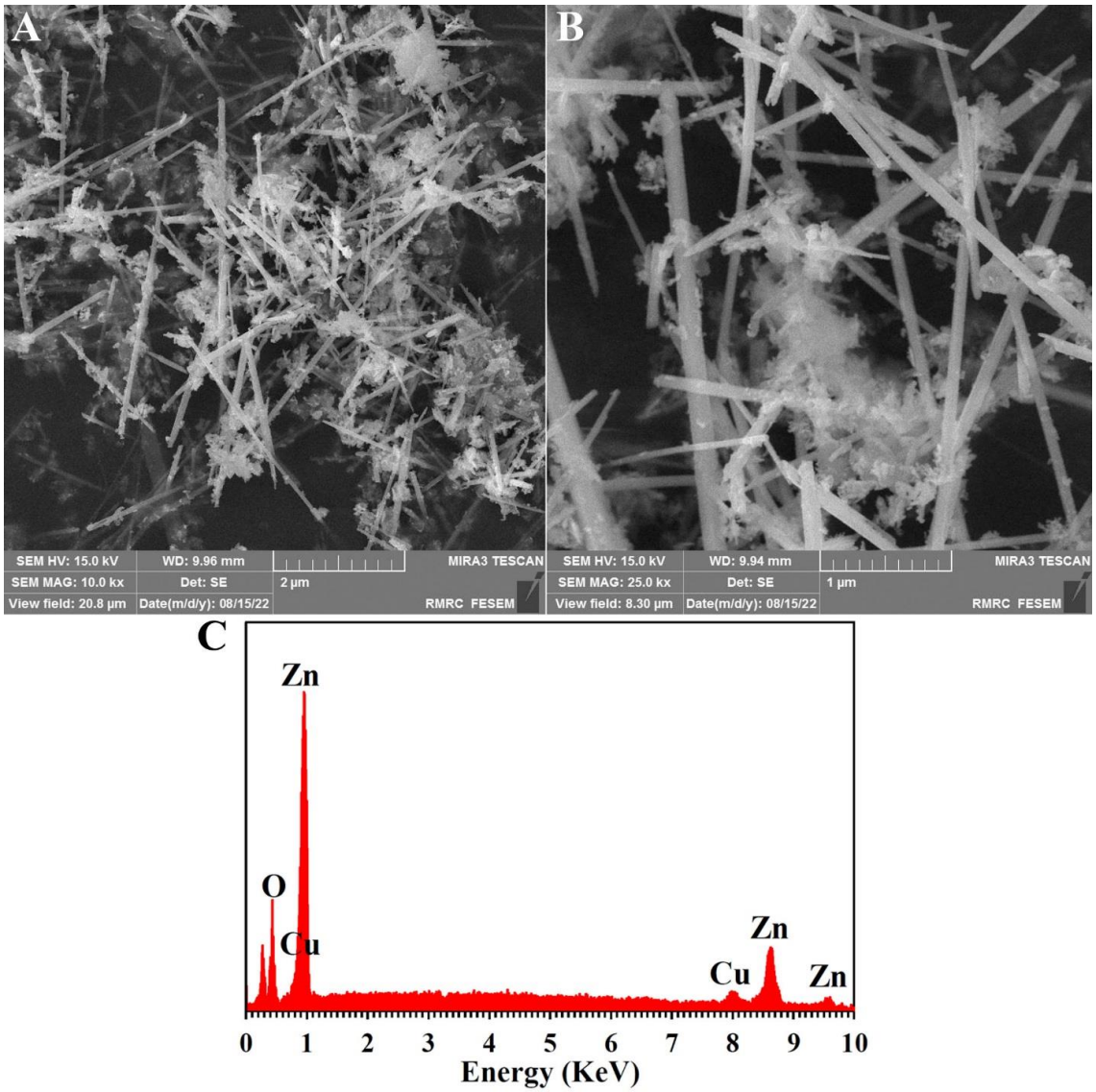

Fig. 2. FE-SEM image (A and B) and EDS spectrum (C) of ZnO-40Cu2O nanocomposite.

limitations of Debye-Scherrer's equation [30].

To confirm the presence of ZnO and Cu_2O compounds in the ZnO-Cu_2O nanocomposite, the EDS analysis was carried out on the ZnO-40Cu_2O sample to identify the elemental composition and to authenticate the presence of Cu_2O and ZnO in this sample. The peaks of Zn, O, and Cu elements are seen in the EDS spectrum of the ZnO-40Cu_2O sample in Fig. 2C, indicating the victorious synthesis of the ZnO-Cu_2O heterojunction. Based on the result of this analysis, the weight percentage of the Zn, O, and Cu elements in the ZnO-40Cu_2O sample are about 54%, 20%, and 26%, respectively. Therefore, it could be concluded that the weight percentage of Cu_2O in this sample is lower than that of the expected 40%, which may be related to the incomplete reaction of the Cu_2O preparation method.

The optical characteristics of the synthesized photocatalysts were studied by UV-Vis diffuse reflectance spectroscopy (UV-DRS) on Shimadzu UV-2550 UV–vis spectrophotometer (Japan). As shown in Fig. 3, the absorption edge of the ZnO nanorods is located at about 400 nm and the absorption edge of the Cu_2O nanoparticles is about 630 nm. Furthermore, compared with ZnO, the absorption edge of the ZnO-Cu_2O nanocomposite has a redshift, therefore compositing of ZnO with

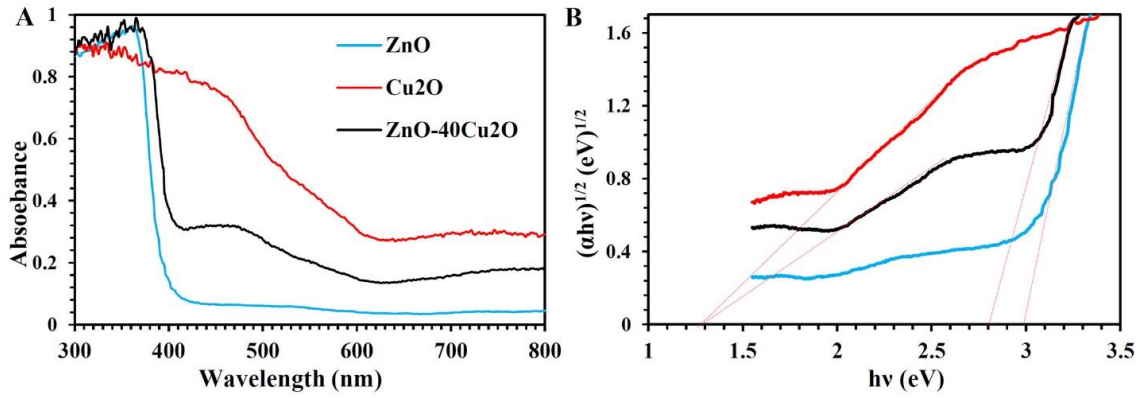

Fig. 3. (a) UV–vis absorption spectra and (b) the plots of $(\alpha h\nu)^{1/2}$ vs hν for obtaining the band gap energy (Eg) of the prepared sample.

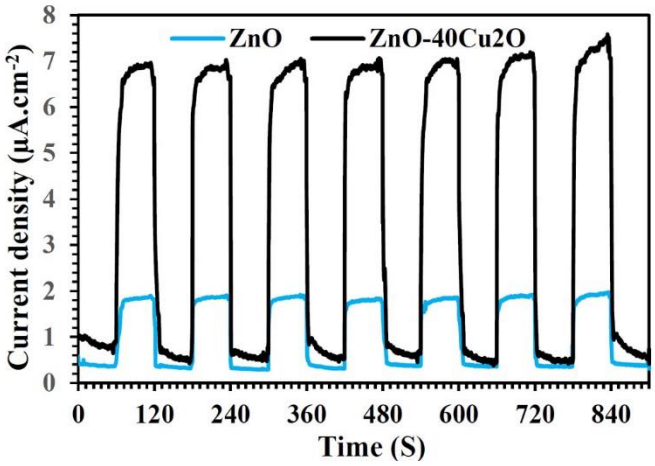

Fig. 4. PL spectra of the prepared samples.

Cu_2O could enhance the visible light harvesting capability of ZnO. The band gap energy (Eg) of the synthesized photocatalysts was estimated by the Kubelka–Munk function [24]. Based on Fig. 3b, the Eg values of ZnO and Cu_2O are about 3 eV and 1.3 eV, respectively. Whereas the ZnO-Cu_2O heterojunction photocatalyst has two Eg values at 2.8 and 1.3 eV, resulting from ZnO and Cu_2O semiconductors. Decreasing the Eg of ZnO confirms the considerable effect of the heterojunction compositing on the narrowing of the ZnO band gap [31], which could result in the enhancement of its visible light absorption capability and visible light photocatalytic efficiency.

The photocurrent analysis could be applied for investigating the charge carriers' separation on the synthesized samples. Any increase in the photocurrent density could be related to the suppression of charge carriers' recombination, which could result in the improvement of the photocatalytic efficiency [32]. As seen in Fig. 4, the photocurrent density of the ZnO-40Cu2O heterojunction nanocomposite is remarkably higher than that of the bare ZnO sample. Therefore, this increase in the photocurrent density could be related to the reduction of the recombination of charge carriers. Therefore, because of the decreasing recombination rate of charge carriers on the ZnO-Cu_2O nanocomposite, this sample could have improved photocatalytic activity.

The potentials of the conduction band edge (E_C) and the valance band edge (E_V) of the ZnO and Cu_2O samples was estimated by the Mott-Schottky experiment, as seen in Fig. 5. The positive slope of the Mott-Schottky plot of the ZnO photocatalyst demonstrates the n-type nature of this semiconductor. But, the negative slope of the Mott-Schottky plot of the Cu_2O sample, indicates that is the p-type nature of Cu_2O [33, 34]. As shown in Fig. 5a and Fig. 5b, the E_{FB} of Cu_2O and ZnO

Table.1. Comparison of the photocatalytic activity of the ZnO-Cu_2O sample with reported results

Photocatalyst	Light	Degradation time	Ref
TiO2 film	Visible	300 min	[37]
Pd/TiO2	Visible	90 min	[38]
La: ZnO/PAN nanofiber	UV	120 min	[39]
UiO-66/g-C3N4	pseudo-sunlight	60 min	[40]
N-doped TiO2 film	Visible	240 min	[41]
ZnO-Cu2O	Visible	180 min	This work

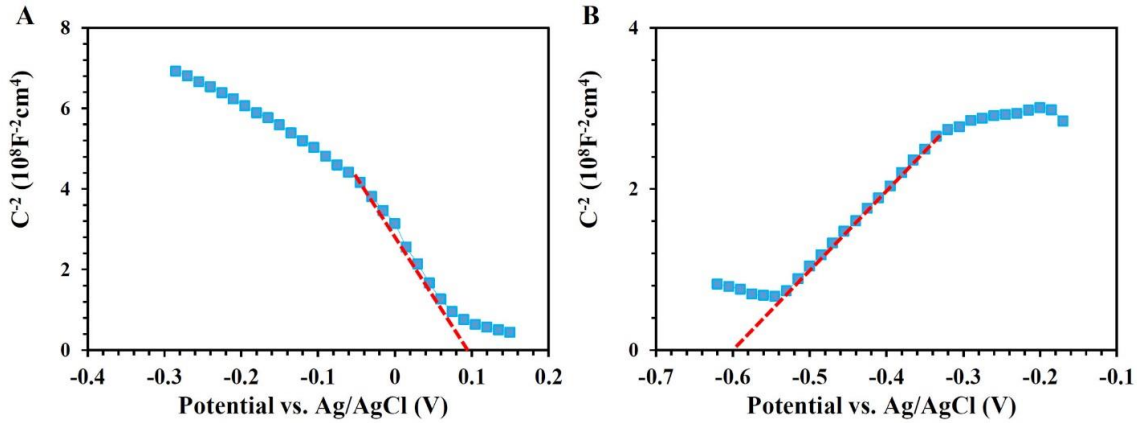

Fig. 5. Mott-Schottky measurements for (A) Cu_2O and (B) ZnO samples.

are around +0.1 V and -0.6 V (vs. Ag/AgCl) (+0.3 V and -0.4 V vs. NHE), respectively. As previously reported, for an n-type semiconductor, the E_{FB} value is 0.1 V lower than the $E_{C,}$ and for a p-type semiconductor, E_{FB} is about ~0.1 eV higher than the E_V [35]. Therefore, the E_C of Cu_2O and ZnO samples are about +0.4 and -0.5 eV vs. NHE, respectively. E_V of Cu_2O and ZnO samples are estimated by $E_V = E_C + Eg$ equation, hence, the E_V of these samples are 0.9 and 2.5 eV vs. NHE, respectively.

The photocatalytic efficiencies of the produced samples were examined by evaluating the photocatalytic degradation of Paraoxon insecticide on the prepared photocatalysts under the irradiation of visible light. As seen in Fig. 6(A), without the addition of any photocatalyst (Blank) sample, Paraoxon is not degraded, indicating its stability under visible light. On the other hand, considerable decomposition is seen in the existence of ZnO and ZnO-Cu_2O heterojunction nanocomposites, and about 100% of Paraoxon is decomposed after 180 min of irradiation, on ZnO-40Cu_2O heterojunction sample with 40% weight percentage of Cu_2O nanoparticles which has the best performance. Because of the enhancement of the visible light harvesting capability and due to the reduction of the electron-hole pairs recombination on the ZnO-Cu_2O samples, these samples have considerably enhanced photocatalytic activity. The kinetics of the photocatalytic degradation reactions of Paraoxon over the prepared photocatalysts were evaluated based on the Pseudo first-order equation (Eq. (1)) according to the Langmuir-Hinshelwood (L–H) model [36].

$$-\ln\left(\frac{C_t}{C_0}\right) = k_{app}t - \ln\left(\frac{C_t}{C_0}\right) = k_{app}t \quad (1)$$

Where $k_{app}k_{app}$ is apparent reaction constant, and C_tC_t and C_0C_0 are the Paraoxon concentrations at illumination time (t) of 0 and t respectively. Fig. 6(B) shows the obtained plots for the photocatalytic decomposition of Paraoxon over the synthesized photocatalysts. $k_{app}k_{app}$ of the ZnO, and ZnO-40Cu_2O samples are measured as 0.0021, and 0.0201 min^{-1}, respectively. Therefore, the existence of Cu_2O

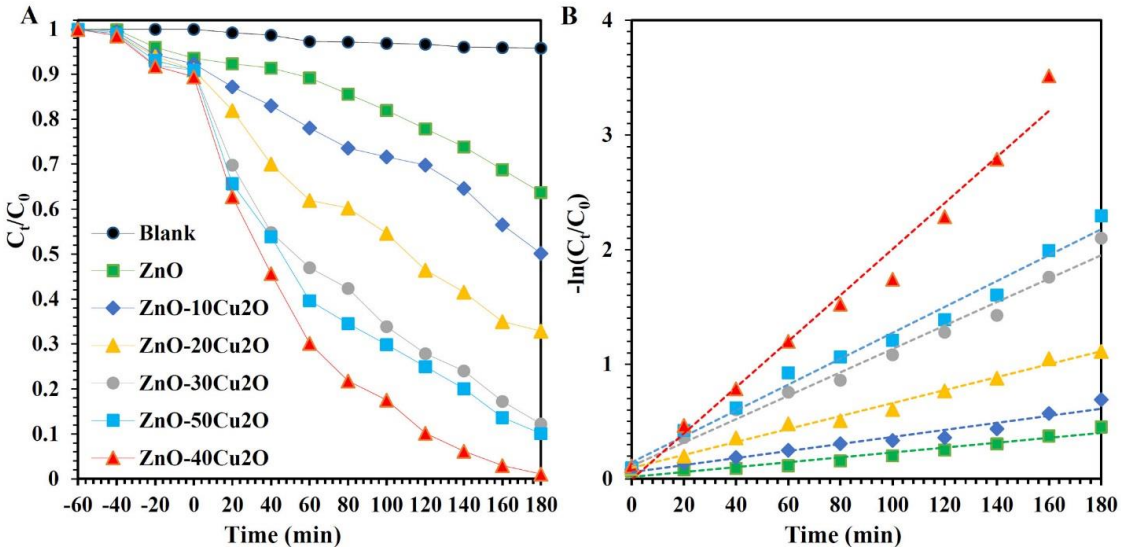

Fig. 6. (A) Visible light photocatalytic degradation of Paraoxon by using the synthesized samples, (B) kinetics of the photocatalytic degradation reactions of Paraoxon based on the Pseudo first-order equation.

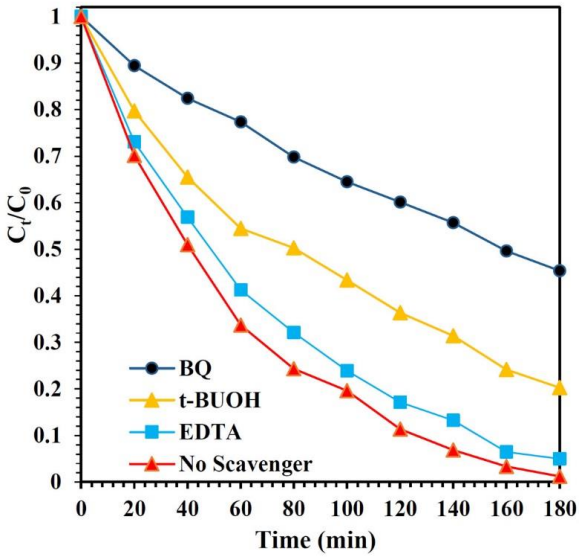

Fig. 7. Activities of ZnO-Cu2O nanocomposite for the visible light photocatalytic decomposition of Paraoxon in the existence of various scavengers

in the ZnO-Cu_2O heterojunction considerably improves the visible light photocatalytic efficiency of ZnO. In table.1 the photocatalytic performance of the ZnO-40Cu_2O heterojunction with previously reported works, as seen in this table this sample has improved photocatalytic performance.

To study the function of hydroxyl radical ($OH^{\bullet}$), superoxide radical ($O_2^{\bullet-}$), and hole, on the photocatalytic degradation of Paraoxon over the ZnO-Cu_2O heterojunction, tert-Butyl alcohol (t-BUOH), benzoquinone (BQ), and Ethylenediaminetetraacetic acid (EDTA) were added into the reaction solution as scavengers of these species, respectively [42]. As seen in Fig. 7 the highest decrease in the photocatalytic performance is observed in presence of benzoquinone, indicating the main function of superoxide radicals for the photocatalytic decomposition of Paraoxon. Furthermore, the photocatalytic degradation is also decreased in presence of t-BUOH. Therefore, hydroxyl and superoxide radicals are the major oxidizing species responsible for the photocatalytic

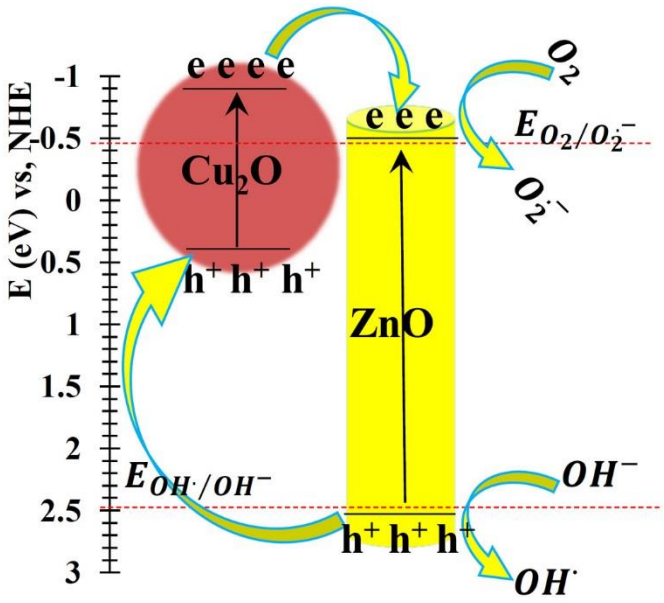

Fig. 8. Type II charge transfer processes for the photocatalytic activity of the ZnO-Cu2O nanocomposite.

activity of ZnO-Cu_2O nanocomposite under visible light illumination.

Fig. 8 indicates a schematic view of the band energy diagram and type II charge transfer processes for the photocatalytic activity of the ZnO-Cu_2O heterojunction photocatalyst, under visible light illumination. With an incidence of visible light photons onto this photocatalyst, the electrons–hole pairs are produced in these semiconductors. The photo-generated electron on the CB of Cu_2O transfers to the CB of ZnO, and simultaneously, the hole on the VB of ZnO transfers to the VB of Cu_2O [43]. Therefore, the recombination of electron–hole pairs is considerably suppressed, and the life span of photoinduced holes and electrons is greatly increased. As a result, more $O_2^{\bullet-}$ and OH radicals are generated, and the oxidation power of the photoinduced electrons and holes is improved, resulting in the enhancement of the photocatalytic performance. According to the acquired results, the following degradation mechanism could be proposed for the degradation of Paraoxon over the ZnO-Cu_2O heterojunction nanocomposite:

$$\text{Paraoxon (aq)} + OH^{\bullet}\,(aq) + O_2^{\bullet-}\,(aq) \xrightarrow[h\nu]{ZnO-Cu2O} CO_2\,(g) + H_2O\,(l) + NO_3^-\,(aq) + PO_4^{3-}\,(aq) \quad (2)$$

CONCLUSION

In the current study, a novel heterojunction nanocomposite was prepared via a hydrothermal route from ZnO nanorods and Cu_2O nanoparticles and was applied for the visible light photocatalytic degradation of Paraoxon insecticide. As the results indicated, the best photocatalytic efficiency was obtained for the ZnO-Cu_2O heterojunction nanocomposite with a 40% weight percentage of Cu_2O nanoparticles which has a photocatalytic activity of 0.0201 min^{-1}. Due to the suppression of the recombination of the photoinduced electron-hole pairs, and enhancement of the visible light harvesting ability, the ZnO-Cu_2O heterojunction has increased photocatalytic activity. Also, based on the Mott-Schottky experiments and the radical trapping tests, a type II charge transfer process was demonstrated for the decomposition of Paraoxon, and superoxide radical was proved as the main active species for the degradation reaction.

CONFLICT OF INTEREST

The authors declare no conflict of interest.

REFERENCES

[1] H. Fu, P. Tan, R. Wang, S. Li, H. Liu, Y. Yang, Z. Wu, Advances in organophosphorus pesticides pollution: Current status and challenges in ecotoxicological, sustainable agriculture, and degradation strategies, Journal of Hazardous Materials, 424 (2022) 127494.

https://doi.org/10.1016/j.jhazmat.2021.127494
[2] P.R.S. Soares, W.G. Birolli, I.M. Ferreira, A.L.M. Porto, Biodegradation pathway of the organophosphate pesticides chlorpyrifos, methyl parathion and profenofos by the marine-derived fungus Aspergillus sydowii CBMAI 935 and its potential for methylation reactions of phenolic compounds, Marine Pollution Bulletin, 166 (2021) 112185. https://doi.org/10.1016/j.marpolbul.2021.112185
[3] X. Wang, Q. Wang, K. Jermsittiparsert, R. Hosseinzadeh, G. Hosseinzadeh, Innovative synthesis of graphene/Pd-doped TiO2 nanocomposite by combination of sonochemical and freeze-drying methods with enhanced visible-light photocatalytic activity, Applied Nanoscience, 10 (2020) 1581-1589. https://doi.org/10.1007/s13204-020-01317-x
[4] X.-h. Wei, C. Li, C. Wang, S. Lin, J. Wu, M.-j. Guo, Rapid and destructive adsorption of paraoxon-ethyl toxin via a self-detoxifying hybrid electrospun nanofibrous membrane, Chemical Engineering Journal, 351 (2018) 31-39. https://doi.org/10.1016/j.cej.2018.06.090
[5] X. Li, J. Xie, C. Jiang, J. Yu, P. Zhang, Review on design and evaluation of environmental photocatalysts, Frontiers of Environmental Science & Engineering, 12 (2018) 1-32. https://doi.org/10.1007/s11783-018-1076-1
[6] H. Wang, X. Li, X. Zhao, C. Li, X. Song, P. Zhang, P. Huo, A review on heterogeneous photocatalysis for environmental remediation: From semiconductors to modification strategies, Chinese Journal of Catalysis, 43 (2022) 178-214. https://doi.org/10.1016/S1872-2067(21)63910-4
[7] M. Shekofteh-Gohari, A. Habibi-Yangjeh, M. Abitorabi, A. Rouhi, Magnetically separable nanocomposites based on ZnO and their applications in photocatalytic processes: a review, Critical Reviews in Environmental Science and Technology, 48 (2018) 806-857. https://doi.org/10.1080/10643389.2018.1487227
[8] S. Majumder, S. Chatterjee, P. Basnet, J. Mukherjee, ZnO based nanomaterials for photocatalytic degradation of aqueous pharmaceutical waste solutions-A contemporary review, Environmental Nanotechnology, Monitoring & Management, 14 (2020) 100386. https://doi.org/10.1016/j.enmm.2020.100386
[9] S. Goktas, A. Goktas, A comparative study on recent progress in efficient ZnO based nanocomposite and heterojunction photocatalysts: A review, Journal of Alloys and Compounds, 863 (2021) 158734. https://doi.org/10.1016/j.jallcom.2021.158734
[10] F. Sanakousar, C. Vidyasagar, V. Jiménez-Pérez, K. Prakash, Recent progress on visible-light-driven metal and non-metal doped ZnO nanostructures for photocatalytic degradation of organic pollutants, Materials Science in Semiconductor Processing, 140 (2022) 106390. https://doi.org/10.1016/j.mssp.2021.106390
[11] W. Xie, Y. Li, W. Sun, J. Huang, H. Xie, X. Zhao, Surface modification of ZnO with Ag improves its photocatalytic efficiency and photostability, Journal of Photochemistry and Photobiology A: chemistry, 216 (2010) 149-155. https://doi.org/10.1016/j.jphotochem.2010.06.032
[12] Y. Lin, H. Hu, Y.H. Hu, Role of ZnO morphology in its reduction and photocatalysis, Applied Surface Science, 502 (2020) 144202. https://doi.org/10.1016/j.apsusc.2019.144202
[13] B. Abebe, H.A. Murthy, E. Amare, Enhancing the photocatalytic efficiency of ZnO: Defects, heterojunction, and optimization, Environmental nanotechnology, monitoring & management, 14 (2020) 100336. https://doi.org/10.1016/j.enmm.2020.100336
[14] G. Hosseinzadeh, S. Zinatloo-Ajabshir, A. Yousefi, Innovative synthesis of a novel ZnO/ZnBi2O4/graphene ternary heterojunction nanocomposite photocatalyst in the presence of tragacanth mucilage as natural surfactant, Ceramics International, 48 (2022) 6078-6086. https://doi.org/10.1016/j.ceramint.2021.11.146
[15] Y.T. Prabhu, V.N. Rao, M.V. Shankar, B. Sreedhar, U. Pal, The facile hydrothermal synthesis of CuO@ZnO heterojunction nanostructures for enhanced photocatalytic hydrogen evolution, New Journal of Chemistry, 43 (2019) 6794-6805. https://doi.org/10.1039/C8NJ06056H
[16] R. Gang, L. Xu, Y. Xia, J. Cai, L. Zhang, S. Wang, R. Li, Fabrication of MoS2 QDs/ZnO nanosheet 0D/2D heterojunction photocatalysts for organic dyes and gaseous heavy metal removal, Journal of Colloid and Interface Science, 579 (2020) 853-861. https://doi.org/10.1016/j.jcis.2020.06.116
[17] B. Liu, C. Bie, Y. Zhang, L. Wang, Y. Li, J. Yu, Hierarchically porous ZnO/g-C3N4 S-scheme heterojunction photocatalyst for efficient H2O2 production, Langmuir, 37 (2021) 14114-14124. https://doi.org/10.1021/acs.langmuir.1c02360
[18] T. Chankhanittha, S. Nanan, Visible-light-driven photocatalytic degradation of ofloxacin (OFL) antibiotic and Rhodamine B (RhB) dye by solvothermally grown ZnO/Bi2MoO6 heterojunction, Journal of Colloid and Interface Science, 582 (2021) 412-427. https://doi.org/10.1016/j.jcis.2020.08.061
[19] P. Xu, P. Wang, Q. Wang, R. Wei, Y. Li, Y. Xin, T. Zheng, L. Hu, X. Wang, G. Zhang, Facile synthesis of Ag2O/ZnO/rGO heterojunction with enhanced photocatalytic activity under simulated solar light: Kinetics and mechanism, Journal of Hazardous Materials, 403 (2021) 124011. https://doi.org/10.1016/j.jhazmat.2020.124011
[20] X. Lu, J.N. Hart, Y. Yao, C.Y. Toe, J. Scott, Y.H. Ng, Cu2O photocatalyst: Activity enhancement driven by concave surface, Materials Today Energy, 16 (2020) 100422. https://doi.org/10.1016/j.mtener.2020.100422
[21] X. Li, S. Raza, C. Liu, Directly electrospinning synthesized Z-scheme heterojunction TiO2@ Ag@ Cu2O nanofibers with enhanced photocatalytic degradation activity under solar light irradiation, Journal of Environmental Chemical Engineering, 9 (2021) 106133. https://doi.org/10.1016/j.jece.2021.106133
[22] A. Guleria, R. Sharma, A. Singh, N.K. Upadhyay, P. Shandilya, Direct dual-Z-scheme PANI/Ag2O/Cu2O heterojunction with broad absorption range for photocatalytic degradation of methylene blue, Journal of Water Process Engineering, 43 (2021) 102305. https://doi.org/10.1016/j.jwpe.2021.102305
[23] R. Zhang, Y. Li, W. Zhang, Y. Sheng, M. Wang, J. Liu, Y. Liu, C. Zhao, K. Zeng, Fabrication of Cu2O/Bi2S3 heterojunction photocatalysts with enhanced visible light photocatalytic mechanism and degradation pathways of tetracycline, Journal of Molecular Structure, 1229 (2021) 129581. https://doi.org/10.1016/j.molstruc.2020.129581
[24] A. Norouzi, A. Nezamzadeh-Ejhieh, α-Fe2O3/Cu2O heterostructure: Brief characterization and kinetic aspect of degradation of methylene blue, Physica B: Condensed Matter, 599 (2020) 412422. https://doi.org/10.1016/j.physb.2020.412422

[25] A. Kumar, S.K. Sharma, G. Sharma, C. Guo, D.-V.N. Vo, J. Iqbal, M. Naushad, F.J. Stadler, Silicate glass matrix@ Cu2O/Cu2V2O7 pn heterojunction for enhanced visible light photo-degradation of sulfamethoxazole: High charge separation and interfacial transfer, Journal of Hazardous Materials, 402 (2021) 123790. https://doi.org/10.1016/j.jhazmat.2020.123790

[26] Y. Xia, Z. He, K. Hu, B. Tang, J. Su, Y. Liu, X. Li, Fabrication of n-SrTiO3/p-Cu2O heterojunction composites with enhanced photocatalytic performance, Journal of Alloys and Compounds, 753 (2018) 356-363. https://doi.org/10.1016/j.jallcom.2018.04.231

[27] X. Men, H. Chen, K. Chang, X. Fang, C. Wu, W. Qin, S. Yin, Three-dimensional free-standing ZnO/graphene composite foam for photocurrent generation and photocatalytic activity, Applied Catalysis B: Environmental, 187 (2016) 367-374. https://doi.org/10.1016/j.apcatb.2016.01.052

[28] S. Tiwari, S. Kumar, A.K. Ganguli, Role of MoS2/rGO co-catalyst to enhance the activity and stability of Cu2O as photocatalyst towards photoelectrochemical water splitting, Journal of Photochemistry and Photobiology A: Chemistry, 424 (2022) 113622. https://doi.org/10.1016/j.jphotochem.2021.113622

[29] U. Holzwarth, N. Gibson, The Scherrer equation versus the'Debye-Scherrer equation', Nature nanotechnology, 6 (2011) 534-534. https://doi.org/10.1038/nnano.2011.145

[30] P. Dauthal, M. Mukhopadhyay, Biosynthesis of palladium nanoparticles using Delonix regia leaf extract and its catalytic activity for nitro-aromatics hydrogenation, Industrial & Engineering Chemistry Research, 52 (2013) 18131-18139. https://doi.org/10.1021/ie403410z

[31] B.-X. Zhou, W.-Q. Huang, K. Yang, S.S. Ding, Z. Xie, A. Pan, W. Hu, P. Peng, G.-F. Huang, Theory-driven heterojunction photocatalyst design with continuously adjustable band gap materials, The Journal of Physical Chemistry C, 122 (2018) 28065-28074. https://doi.org/10.1021/acs.jpcc.8b08060

[32] D.V. Markovskaya, A.V. Zhurenok, S.V. Cherepanova, E.A. Kozlova, Solid solutions of CdS and ZnS: Comparing photocatalytic activity and photocurrent generation, Applied Surface Science Advances, 4 (2021) 100076. https://doi.org/10.1016/j.apsadv.2021.100076

[33] Z. Dong, J. Zhou, Z. Zhang, Y. Jiang, R. Zhou, C. Yao, Construction of a p-n Type S-Scheme Heterojunction by Incorporating CsPbBr3 Nanocrystals into Mesoporous Cu2O Microspheres for Efficient CO2 Photoreduction, ACS Applied Energy Materials, 5 (2022) 10076-10085. https://doi.org/10.1021/acsaem.2c01760

[34] A. Bahadoran, S. Masudy-Panah, J.R. De Lile, J. Li, J. Gu, B. Sadeghi, S. Ramakrishna, Q. Liu, Novel 0D/1D ZnBi2O4/ZnO S-scheme photocatalyst for hydrogen production and BPA removal, International Journal of Hydrogen Energy, 46 (2021) 24094-24106. https://doi.org/10.1016/j.ijhydene.2021.04.208

[35] Y. Cao, A. El-Shafay, A.H. Mohammed, S.F. Almojil, A.I. Almohana, A.F. Alali, Controlling the charge carriers recombination kinetics on the g-C3N4-BiSI nn heterojunction with efficient photocatalytic activity in N2 fixation and degradation of MB and phenol, Advanced Powder Technology, 33 (2022) 103513. https://doi.org/10.1016/j.apt.2022.103513

[36] M. Saeed, I. Khan, M. Adeel, N. Akram, M. Muneer, Synthesis of a CoO-ZnO photocatalyst for enhanced visible-light assisted photodegradation of methylene blue, New Journal of Chemistry, 46 (2022) 2224-2231. https://doi.org/10.1039/D1NJ05633F

[37] G. Prasad, P. Ramacharyulu, J.P. Kumar, A. Srivastava, B. Singh, Photocatalytic degradation of paraoxon-ethyl in aqueous solution using titania nanoparticulate film, Thin Solid Films, 520 (2012) 5597-5601. https://doi.org/10.1016/j.tsf.2012.04.033

[38] A.H. Keihan, H. Rasoulnezhad, A. Mohammadgholi, S. Sajjadi, R. Hosseinzadeh, M. Farhadian, G. Hosseinzadeh, Pd nanoparticle loaded TiO2 semiconductor for photocatalytic degradation of Paraoxon pesticide under visible-light irradiation, Journal of materials science: materials in electronics, 28 (2017) 16718-16727. https://doi.org/10.1007/s10854-017-7585-z

[39] K. Lakshmi, K. Kadirvelu, P.S. Mohan, Reclaimable La: ZnO/PAN nanofiber catalyst for photodegradation of methyl paraoxon and its toxicological evaluation utilizing early life stages of zebra fish (Danio rerio), Chemical Engineering Journal, 357 (2019) 724-736. https://doi.org/10.1016/j.cej.2018.09.201

[40] D. Van Le, M.B. Nguyen, P.T. Dang, T. Lee, T.D. Nguyen, Synthesis of a UiO-66/gC 3 N 4 composite using terephthalic acid obtained from waste plastic for the photocatalytic degradation of the chemical warfare agent simulant, methyl paraoxon, RSC advances, 12 (2022) 22367-22376. https://doi.org/10.1039/D2RA03483B

[41] H. Rasoulnezhad, G. Hosseinzadeh, R. Hosseinzadeh, N. Ghasemian, Preparation of transparent nanostructured N-doped TiO2 thin films by combination of sonochemical and CVD methods with visible light photocatalytic activity, Journal of Advanced Ceramics, 7 (2018) 185-196. https://doi.org/10.1007/s40145-018-0270-8

[42] R. Elshypany, H. Selim, K. Zakaria, A.H. Moustafa, S.A. Sadeek, S. Sharaa, P. Raynaud, A.A. Nada, Elaboration of Fe3O4/ZnO nanocomposite with highly performance photocatalytic activity for degradation methylene blue under visible light irradiation, Environmental Technology & Innovation, 23 (2021) 101710. https://doi.org/10.1016/j.eti.2021.101710

[43] J. Xue, J. Bao, Interfacial charge transfer of heterojunction photocatalysts: Characterization and calculation, Surfaces and Interfaces, 25 (2021) 101265. https://doi.org/10.1016/j.surfin.2021.101265